ACADEMIC PRESS

Available online at www.sciencedirect.com
SCIENCE DIRECT®

Journal of Colloid and Interface Science 263 (2003) 288–295

JOURNAL OF Colloid and Interface Science

www.elsevier.com/locate/jcis

Effective velocity and effective dispersion coefficient for finite-sized particles flowing in a uniform fracture

Scott C. James *,[1] and Constantinos V. Chrysikopoulos

Department of Civil and Environmental Engineering, University of California, Irvine, CA 92697-2175, USA

Received 19 June 2002; accepted 5 March 2003

Abstract

In this work we derive expressions for the effective velocity and effective dispersion coefficient for finite-sized spherical particles with neutral buoyancy flowing within a water saturated fracture. We considered the miscible displacement of a fluid initially free of particles by another fluid containing particles of finite size in suspension within a fracture formed by two semi-infinite parallel plates. Particle spreading occurs due to the combined actions of molecular diffusion and the dispersive effect of the Poiseuille velocity profile. Unlike Taylor dispersion, here the finite size of the particles is taken into account. It is shown that because the finite size of a particle excludes it from the slowest moving portion of the velocity profile, the effective particle velocity is increased, while the overall particle dispersion is reduced. A similar derivation applied to particles flowing in uniform tubes yields analogous results. The effective velocity and dispersion coefficient derived in this work for particle transport in fractures with uniform aperture are unique and ideally suited for use in particle tracking models.

Keywords: Effective parameters; Polydisperse; Colloids; Transport; Uniform aperture fracture

1. Introduction

Sir Geoffrey Taylor [1] introduced an effective dispersion coefficient for soluble matter flowing in a cylindrical tube. Often referred to as the Taylor dispersion coefficient, it is a function of the dissolved constituent's molecular diffusion coefficient and the fundamental system parameters (i.e., centerline flow velocity and tube radius). Aris [2] extended this work through moment analysis in a more generalized manner. Sankarasubramanian and Gill [3], Johns and DeGance [4], and Brenner [5,6] continued the study of internal flow and transport by developing exact solutions for the dispersion of reactive solutes in a tube. Following the Taylor–Aris procedures, scientists have examined various aspects of contaminant transport in parallel-plate systems. For example, Shapiro and Brenner [7–9] and Berkowitz and Zhou [10] have obtained approximate analytical models for the dispersion of reactive solutes in parallel-plate geometries and concluded that the Taylor dispersion coefficient needs to be modified to account for system geometry and for particle flux at system boundaries due to wall reactions. Effective parameters were also derived by Grindrod [11,12] using an asymptotic spectral comparison method. Other important contributions include analytical solutions for contaminant transport in fractured porous media, where contaminants are subject to plug flow advection, dispersion, matrix diffusion, sorption, and decay (Tang et al. [13]; Sudicky and Frind [14]; Cormenzana [15]). Also, Abdel-Salam and Chrysikopoulos [16] derived closed-form analytical solutions for contaminant transport in single, uniform rock fractures with and without penetration into the rock matrix for constant concentration as well as constant flux boundary conditions.

It is often assumed that solutes are infinitesimally small and that axial advection and transverse diffusion chiefly govern contaminant fate and transport in fractures. While it is true that many contaminants are of molecular size, this is not always the case (Chrysikopoulos and Abdel-Salam [17]). Many studies have shown colloids to be ubiquitous in groundwater while often having an affinity for reactive contaminants (Smith and Degueldre [18]; Contardi et al. [19]). Essentially, if a contaminant sorbs onto a colloid, the colloid itself becomes a contaminant (Abdel-Salam and Chrysikopoulos [20,21]).

* Corresponding author.
E-mail address: scjames@sandia.gov (S.C. James).
[1] Present address: Sandia National Laboratories, Geohydrology Department, P.O. Box 5800, Albuquerque, NM 87185-0735, USA.

0021-9797/03/$ – see front matter
doi:10.1016/S0021-9797(03)00254-6

Much of the groundwork for the development of the effective parameters for finite particles flowing in a fracture was based upon particle flow and transport in a tube. Although the solution of Brenner and Gaydos [22] is quite broad in nature, it is difficult to implement in a model of colloid transport in fractured media. Often, there is insufficient information about colloidal interactions with the fluid or medium to accurately define the coefficients in their effective parameters. In this work, the effective velocity and effective dispersion coefficient for finite-sized, hard, spherical colloidal particles with neutral buoyancy are derived from first principles in an intuitive fashion. It is shown that the finite size of a particle excludes it from the slowest moving portion of the velocity profile near the walls of a fracture, causing the effective velocity of a particle plume to be greater than the corresponding mean solute velocity. Furthermore, particle size exclusion leads to a decrease in the effective dispersion coefficient of a particle plume. When used in a particle tracking algorithm, excellent agreement with an analytical solution is demonstrated.

2. Mathematical derivations

2.1. Effective velocity

Assume that a fully developed, unidimensional, Poiseuille velocity distribution exists within a fracture as shown in Fig. 1, expressed as (Fox and McDonald [23, p. 392])

$$u(z) = U_{\max}\left[1 - 4\left(\frac{z}{b}\right)^2\right]. \tag{1}$$

The mean fluid velocity is

$$\overline{U} = \frac{1}{b}\int_{-b/2}^{b/2} u(z)\,dz = \frac{2}{3}U_{\max}, \tag{2}$$

where $U_{\max}$ is the maximum velocity of the interstitial fluid along the centerline of the fracture; z is the coordinate direction perpendicular to the walls of the fracture with its origin at the center of the fracture; and b is the aperture of the fracture. Furthermore, assume that a spherical particle travels

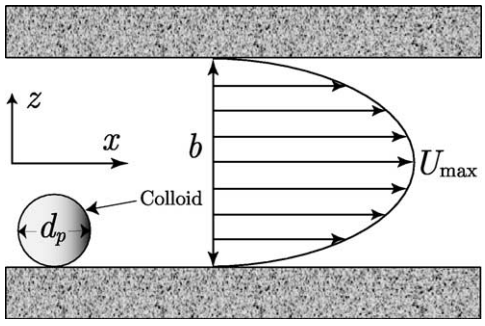

Fig. 1. Schematic illustration of the fracture considered in this study.

with a velocity corresponding to the local flow velocity at its centroid. Particle–wall overlap is not allowed. Hydrodynamic, gravitational, van der Waals, and electrostatic forces are not considered in the calculation of particle velocity. As particle penetration of the fracture wall is not permitted, the finite size of a particle does not allow it to sample the slowest moving portion of the velocity profile nearest the wall. The average (or effective) velocity of a particle is estimated by integrating the Poiseuille velocity distribution over the aperture available to a particle and dividing by that same available aperture. The available aperture is the original aperture, b, less the diameter of a particle, d_p. Size exclusion leads to an effective particle velocity of

$$\begin{aligned} U_{\text{eff}} &= \frac{U_{\max}}{b-d_p}\int_{(-b+d_p)/2}^{(b-d_p)/2}\left[1 - 4\left(\frac{z}{b}\right)^2\right]dz \\ &= \frac{2}{3}U_{\max}\left[1 + \frac{d_p}{b} - \frac{1}{2}\left(\frac{d_p}{b}\right)^2\right]. \end{aligned} \tag{3}$$

Note that the effective particle velocity (3) is greater than the mean fluid velocity (2) because the particle diameter may not be larger than the fracture aperture ($d_p/b < 1$). Also, it is evident that the effective velocity of a particle increases with increasing particle diameter.

2.2. Effective dispersion coefficient

The two-dimensional, unsteady, advection–diffusion equation with axial advection and transverse diffusion representing the two governing transport mechanisms is (Berkowitz and Zhou [10])

$$\frac{\partial n(x,z,t)}{\partial t} = \mathcal{D}\frac{\partial^2 n(x,z,t)}{\partial z^2} - u(z)\frac{\partial n(x,z,t)}{\partial x}, \tag{4}$$

where n is the number concentration of colloids and $\mathcal{D}$ is the molecular diffusion coefficient of a particle with diameter d_p, given by the Stokes–Einstein diffusion equation (Bird et al. [24, p. 513]),

$$\mathcal{D} = \frac{kT}{3\pi\eta d_p}, \tag{5}$$

where k is Boltzmann's constant, T is the absolute temperature, and η is the dynamic viscosity of the interstitial fluid.

In the present derivation, the molecular diffusion in the axial direction is neglected because it is negligible relative to the axial dispersion due to the parabolic velocity profile. All axial particle movement is due to advection. A quasi-steady-state assumption is made by considering only advection across the plane moving with the center of mass of a colloid particle plume such that x and t may be collapsed into a single coordinate thereby eliminating transient term in (4). This can be achieved by the coordinate transformation

$$\xi = x - U_{\text{eff}}t. \tag{6}$$

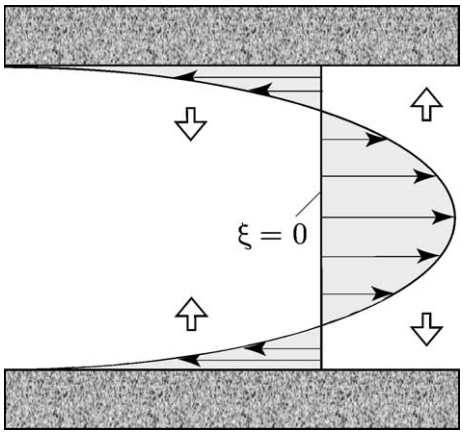

Fig. 2. Schematic illustration of the "velocity defect" represented by the shaded areas. Bold arrows indicate axial advection of particles and open arrows indicate transverse molecular diffusion of particles.

Applying the preceding coordinate transformation in (4) yields the partial differential equation

$$\mathcal{D}\frac{\partial^2 n(\xi,z)}{\partial z^2} = \big[u(z) - U_{\text{eff}}\big]\frac{\partial n(\xi,z)}{\partial \xi}, \tag{7}$$

where the term $u(z) - U_{\text{eff}} = u_\xi(z)$ is termed the "velocity defect," defined as the velocity that is a function of z at a point $\xi = 0$ that follows the first moment of a particle plume in time. Subtracting the effective velocity (3) from the Poiseuille (parabolic) velocity profile (1) yields

$$u_\xi(z) = u(z) - U_{\text{eff}} = \frac{U_{\max}}{3}\left[\left(1-\frac{d_p}{b}\right)^2 - 12\left(\frac{z}{b}\right)^2\right]. \tag{8}$$

Figure 2 illustrates the velocity defect. Note that particles in the shaded regions have a tendency to diffuse in the direction of the open arrows because of the concentration gradient induced by the velocity defect. It is in these shaded regions where axial particle advection (indicated by the bold arrows) and transverse particle diffusion (indicated by the open arrows) are important. With respect to the moving frame of reference, the velocity of a particle that is in contact with the wall is negative: $u_\xi((b-d_p)/2) = -(2/3)U_{\max}(1-d_p/b)^2$. Consequently, the apparent velocity of the particles in the shaded areas to the left of the moving frame of reference is negative as indicated by the direction of the bold arrows. Because the mean particle velocity at the plane for which $\xi = 0$ is zero, the transfer of particles across this plane depends only on the transverse variation of n. In view of (8), the governing equation (7) can be expressed as

$$\frac{\partial^2 n(\xi,z)}{\partial z^2} = \frac{U_{\max}}{3\mathcal{D}}\left[\left(1-\frac{d_p}{b}\right)^2 - 12\left(\frac{z}{b}\right)^2\right]\frac{\partial n(\xi,z)}{\partial \xi}. \tag{9}$$

Employing the assumption that transverse concentration gradients induced by axial advection are quickly smoothed out by transverse molecular diffusion after the frame of reference has moved beyond an "entrance length" (Kessler and Hunt [25, Eq. (11)]), the rate of change of the particle number concentration with respect to the moving frame of reference can be assumed to be nearly constant across the aperture of the fracture. This assumption implies that $\partial n(\xi,z)/\partial\xi$ may be replaced with $\partial n(\xi)/\partial\xi$. Integration of (9) with respect to z yields

$$\frac{\partial n(\xi,z)}{\partial z} = \frac{U_{\max} b}{3\mathcal{D}}\left[\left(1-\frac{d_p}{b}\right)^2\frac{z}{b} - 4\left(\frac{z}{b}\right)^3\right]\frac{\partial n(\xi)}{\partial \xi} + C(\xi), \tag{10}$$

where $C(\xi)$ is an integration constant. Imposing the nondispersive flux boundary condition across the centerline ($z = 0$) because of neutral particle buoyancy requires that the integration constant vanish:

$$\left.\frac{\partial n(\xi,z)}{\partial z}\right|_{z=0} = 0 \Rightarrow C(\xi) = 0. \tag{11}$$

Integration of (10) with respect to z yields

$$n(\xi,z) = \frac{U_{\max} b^2}{6\mathcal{D}}\left[\left(1-\frac{d_p}{b}\right)^2\left(\frac{z}{b}\right)^2 - 2\left(\frac{z}{b}\right)^4\right]\frac{\partial n(\xi)}{\partial \xi} + n_{\text{cl}}(\xi), \tag{12}$$

where $n_{\text{cl}}(\xi)$ is an integration constant. Note that evaluating $n(\xi,0)$ proves that $n_{\text{cl}}(\xi)$ is actually the particle concentration at the centerline of the fracture.

The average particle concentration in the z-direction over the entire fracture aperture is defined by integrating the particle number concentration across the fracture and dividing by the fracture aperture:

$$\bar{n}(\xi) = \frac{1}{b}\int_{-b/2}^{b/2} n(\xi,z)\,dz. \tag{13}$$

Substituting (12) into (13) and performing the integration, the average colloid concentration is

$$\bar{n}(\xi) = \frac{U_{\max} b^2}{6\mathcal{D}}\left[\frac{7}{120} - \frac{1}{6}\frac{d_p}{b} + \frac{1}{12}\left(\frac{d_p}{b}\right)^2\right]\frac{\partial \bar{n}(\xi)}{\partial \xi} + n_{\text{cl}}(\xi). \tag{14}$$

Note that due to averaging over b, the term $\partial n(\xi)/\partial\xi$ can be replaced by $\partial\bar{n}(\xi)/\partial\xi$. Solving (14) for $n_{\text{cl}}(\xi)$ and substituting the resulting expression into (12) defines $n(\xi,z)$ in terms of the average concentration across the fracture:

$$n(\xi,z) = \frac{U_{\max} b^2}{6\mathcal{D}}\left[-\frac{7}{120} + \frac{1}{6}\frac{d_p}{b} - \frac{1}{12}\left(\frac{d_p}{b}\right)^2 + \left(1-\frac{d_p}{b}\right)^2\left(\frac{z}{b}\right)^2 - 2\left(\frac{z}{b}\right)^4\right]\frac{\partial \bar{n}(\xi)}{\partial \xi} + \bar{n}(\xi). \tag{15}$$

The effective dispersion coefficient is derived from the flux of particles across a plane that is moving with the first moment of the particle plume in time. The average flux of

particles in the axial direction relative to the moving coordinate, ξ, is given by

$$\bar{J} = \frac{1}{b-d_p}\int_{(-b+d_p)/2}^{(b-d_p)/2} n(\xi,z)u_\xi(z)\,dz$$
$$= -\frac{2}{945}\frac{U_{\max}^2 b^2}{\mathcal{D}}\left(1-\frac{d_p}{b}\right)^6\frac{\partial\bar{n}(\xi)}{\partial\xi}, \tag{16}$$

where the latter transformation is a consequence of employing (8) and (15). The average flux is calculated only for the portion of the fracture available to the particles, hence the region spanned by the limits of integration.

Using the effective velocity as a moving frame of reference, the transport of particles within the fracture may be viewed as a dispersion problem. Consequently, the advection–diffusion equation may now be redefined as Fick's second law of diffusion along the moving frame of reference, ξ, with diffusion coefficient D_{eff}. Thus, the unsteady transport of particles can be expressed through use of the continuity equation assuming there is no particle generation (Bird et al. [24, p. 555]),

$$\frac{\partial\bar{n}(\xi)}{\partial t} = -\frac{\partial\bar{J}}{\partial\xi}. \tag{17}$$

Substituting the expression for average particle flux (16) into the preceding equation yields

$$\frac{\partial\bar{n}(\xi)}{\partial t} = D_{\text{eff}}\frac{\partial^2\bar{n}(\xi)}{\partial\xi^2}, \tag{18}$$

where the effective dispersion coefficient, D_{eff}, represents the apparent particle spreading arising from the combined effect of the advective flux of particles across the plane moving with the center of mass of a particle plume plus molecular diffusion. It is defined as

$$D_{\text{eff}} = \mathcal{D} + \frac{2}{945}\frac{U_{\max}^2 b^2}{\mathcal{D}}\left(1-\frac{d_p}{b}\right)^6. \tag{19}$$

For the limiting case where a particle becomes negligibly small, $d_p \to 0$, the preceding expression for the effective dispersion coefficient for finitely sized particles reduces to the classic Taylor dispersion coefficient

$$D_{\text{Taylor}} = \mathcal{D} + \frac{2}{945}\frac{U_{\max}^2 b^2}{\mathcal{D}}. \tag{20}$$

3. Discussion

Figure 3 compares the effective dispersion coefficient for particles using (19) to an equivalent Taylor dispersion coefficient, (20). It should be noted that the molecular diffusion coefficient used in both the effective and Taylor dispersion coefficients was calculated from (5), even though the Taylor dispersion coefficient assumes infinitesimally small particles. Figure 3 demonstrates that when the particle diameter is 6.5% of the fracture aperture, the effective dispersion coefficient of the particle plume is 50% less than the corresponding Taylor dispersion coefficient.

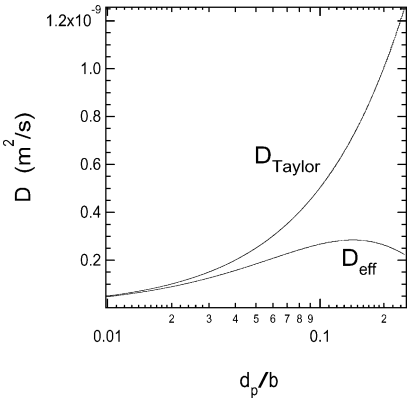

Fig. 3. Effective and Taylor dispersion coefficients as a function of particle-diameter-to-fracture-aperture ratio. The fracture is representative of what might be found in the subsurface with $b = 1 \times 10^{-4}$ m, $U_{\max} = 1 \times 10^{-6}$ m/s, at $T = 288.15$ K.

The limiting cases where the particle diameter becomes infinitesimally small ($d_p \to 0$) as well as when the particle diameter is comparable to the fracture aperture ($d_p \to b$) are also examined. As the diameter of a particle becomes infinitesimally small, the effective velocity with which the particle plume travels is reduced to the mean flow velocity, $U_{\text{eff}} = \frac{2}{3}U_{\max}$ and $D_{\text{eff}} = D_{\text{Taylor}}$. This is in agreement with the assumption of an infinitesimally small solute made by Taylor in his derivation. At the limit of the particle diameter approaching the fracture aperture, the effective velocity of a particle plume becomes $U_{\max}$ while the corresponding effective dispersion coefficient reduces to the molecular diffusion coefficient. Both results arise directly from the assumptions that each particle is assumed to travel with a velocity equal to that found at its centroid due to the hydraulic gradient and that particle–wall overlap is not permitted. An increased particle diameter to fracture aperture ratio implies a narrower range of velocities for a colloid plume, thereby decreasing the dispersive effect of the velocity gradient. If a plume is subject to a single velocity, it spreads by molecular diffusion alone. The expected behavior of D_{eff} at both limits of small and large particles is evident from (19).

Clearly, particle size should be considered when investigating the transport of finite-sized particles through a water-saturated fracture. It should be noted that there have been other derivations of effective velocity and dispersion coefficients for solutes and particles in cylindrical and planar systems (DiMarzio and Guttman [26]; Anderson and Quinn [27]; Brenner and Gaydos [22]); however, the results presented in this study are directly applicable to colloid transport in a uniform aperture fracture.

4. Effects of viscous forces

Although the effects of the fracture walls upon colloid motion have not been addressed thus far, it is important to

note that as a colloid approaches a wall (its surface less than a few diameters away), significant changes in velocity and diffusivity are noted. Specifically, the velocity and diffusivity parallel and perpendicular to the wall decrease in different proportions (i.e., diffusion is no longer isotropic and because the colloid may not penetrate the wall, its perpendicular velocity must approach zero as it nears the wall, while parallel velocity is reduced) (van de Ven [28, Eq. (6.13)]). Unfortunately, these effects may not be incorporated into the analytical derivation presented above, although more complicated solution approximations exist (e.g., method of reflections, matched asymptotic solutions for "inner" and "outer" regions, and truncated power series expansions by Goldman et al. [29], O'Neill and Stewartson [30], and Goren and O'Neill [31], respectively). In this treatment of effective parameters, if the constants $U_{\max}$ and $\mathcal{D}$ are replaced with simple symmetric (even) functions, $U_{\max}(z)$ and $\mathcal{D}(z)$, respectively, the wall effects may be estimated. However, unless the colloid is larger than 10% of the aperture, edge effects are negligible through more than 90% of the fracture, yet very near to the walls, they are significant. Without breaking the solution space into different zones, no simple integrable function can express the correction factor appropriately. For example, a nonanalytically integrable exponential representation of the hydrodynamic correction factor is

$$F(z) = 1 + \alpha - \alpha \exp\left[-\left(\frac{2z}{b - d_p}\right)^{\beta}\right], \tag{21}$$

where α (real) and β (large, positive, and even) are constants that are calculated to match the curves of van de Ven [28, Fig. 6.4]. Although the preceding correction factors may not be carried through the analytical treatment of effective parameters, a numerical solution exists. While this numerical treatment of effective parameters is beyond the scope of this work, incorporating wall effects through (21) would serve to decrease U_{eff} and D_{eff}. Any symmetric equation that approximates the hydrodynamic correction factors may be used and therefore (21) should not be considered unique.

5. Extension to flow in cylindrical tubes

5.1. Mathematical derivation

To extend our results to finite-sized particles flowing in a cylindrical tube, a derivation equivalent to that performed in Cartesian coordinates was performed in cylindrical coordinates. The Poiseuille velocity profile in a tube of radius R is

$$u(r) = U_{\max}\left[1 - \left(\frac{r}{R}\right)^2\right], \tag{22}$$

where r is the radial distance from the center of the tube. The mean velocity within the tube is $\overline{U} = U_{\max}/2$ and the effective velocity of a finite-sized particle is

$$U_{\text{eff}} = \frac{1}{2}U_{\max}\left[1 + \frac{d_p}{R} - \frac{1}{4}\left(\frac{d_p}{R}\right)^2\right]. \tag{23}$$

The governing equation for particle transport in a tube is

$$\frac{\partial n(r,z,t)}{\partial t} = \frac{\mathcal{D}}{r}\frac{\partial}{\partial r}\left[r\frac{\partial n(r,z,t)}{\partial r}\right] - u(r)\frac{\partial n(r,z,t)}{\partial z}. \tag{24}$$

Following the same procedures used to derive the effective dispersivity of a particle in a fracture (see Section 2.2), the effective dispersion coefficient in a uniform tube is

$$D_{\text{eff}} = \mathcal{D} + \frac{1}{192}\frac{U_{\max}^2 R^2}{\mathcal{D}}\left(1 - \frac{d_p}{R}\right)^6. \tag{25}$$

Again, for infinitely small particles, (23) and (25) are in complete accord with the results of Taylor [1].

5.2. Comparison to other studies

DiMarzio and Guttman [26] investigated the case of flexible polymers flowing through a gel permeation column accounting for some hydrodynamic wall effects and derived an expression for the effective velocity equivalent to (23) and an expression for the effective dispersion coefficient that is equivalent to (25).

Anderson and Quinn [27] derived the following expression for the effective velocity of a submicrometer particle passing through a porous membrane,

$$U_{\text{eff}} = \frac{1}{2}U_{\max}\left[1 + \frac{d_p}{R} - \frac{1}{4}\left(\frac{d_p}{R}\right)^2\right] \times \left[1 - \frac{1}{6}\frac{d_p}{R} - 0.02\left(\frac{d_p}{R}\right)^3\right], \tag{26}$$

but they did not determine an equation for the effective dispersion coefficient.

Brenner and Gaydos [22] performed a comprehensive moment analysis to obtain effective parameters of

$$U_{\text{eff}} = \frac{1}{2}U_{\max}\left[1 + \frac{d_p}{R} - 1.225\left(\frac{d_p}{R}\right)^2 + O\left(d_p^2\right)\right] \tag{27}$$

and

$$D_{\text{eff}} = \mathcal{D}\left[1 + 0.231\left(\frac{d_p}{R}\right) - \frac{9}{16}\left(\frac{d_p}{R}\right)\ln\left(\frac{2R}{d_p}\right) - \frac{9}{16}\left(\frac{d_p}{R}\right)^2\ln\left(\frac{2R}{d_p}\right) + O\left(d_p^2\right)\right] + \frac{1}{192}\frac{U_{\max}^2 R^2}{\mathcal{D}}\left[1 - 0.931\left(\frac{d_p}{R}\right) + 2.42\left(\frac{d_p}{R}\right)^2 + O\left(d_p^2\right)\right], \tag{28}$$

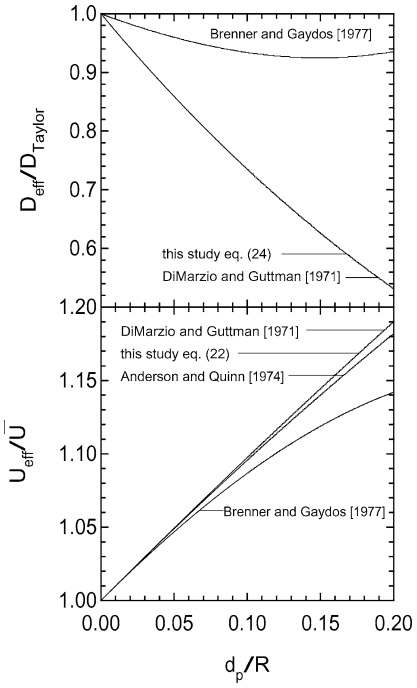

Fig. 4. Comparison of the effective parameters derived in this study with appropriate parameters reported in previous studies. The top plot relates the ratio of effective dispersion to Taylor dispersion as a function of particle to tube diameter ratio. The bottom plot illustrates the relationship between the ratio of the effective velocity to the mean flow velocity and the ratio of particle to tube diameter.

with coefficients incorporating the effects of London, van der Walls, viscous, and Debye double layer forces. Note that, to first order, the expressions (23) and (25) derived here compare well with those of Brenner and Gaydos [22].

Figure 4 compares expressions (23) and (25) with the corresponding expressions derived by DiMarzio and Guttman [26], Anderson and Quinn [27], and Brenner and Gaydos [22]. Clearly, the various results are somewhat different; however, they indicate that the overall trend for finite-sized particles is faster travel and decreased dispersion with increasing particle size. Certainly, the expressions derived by Brenner and Gaydos [22] are most general, but obtaining the coefficients in their equations requires more information than just the particle size and the diameter of the cylinder. Of importance is to note that the expression (28) for the effective dispersion coefficient derived by Brenner and Gaydos [22] goes through a minimum at $d_p/R = 0.149$ and surpasses the Taylor dispersion coefficient at $d_p/R = 0.277$. Theoretically, Taylor dispersion represents the upper limit of dispersion in a tube.

All of the previous studies discussed in this section focus only on particle transport in cylindrical tubes. To our knowledge, the effective parameters (3) and (19) derived in this work for particle transport in water-saturated fractures with uniform aperture are unique. Furthermore, they are easily implemented in particle-tracking algorithms while requiring knowledge only of the fracture aperture and particle diameter.

6. Particle tracking analysis

To further illustrate the effect of particle size on particle transport in a uniform, water-saturated fracture, particle-tracking simulations were conducted. Particle-tracking algorithms are stochastic solutions to linear partial differential equations that do not provide direct numerical solutions and therefore do not suffer from numerical dispersion as do the finite element and finite difference methods. Each particle is individually considered (i.e., stored in a memory location), thus retaining its own unique characteristics including, for example, particle diameter.

Particle-tracking techniques have frequently been applied to investigations of contaminant transport in porous and fractured media (Chrysikopoulos et al. [32]; Thompson et al. [33]; James and Chrysikopoulos [34–36]; Reimus and James [37]; Chrysikopoulos and James [38]). The general particle tracking transport equation consists of an absolute term, in this case due to advection; and a stochastic term representing dispersion in the system (Kitanidis [39]). In vector notation the particle-tracking equation is given by (Thompson and Gelhar [40])

$$\mathbf{X}^m = \mathbf{X}^{m-1} + \mathbf{A}(\mathbf{X}^{m-1})\Delta t + \mathbf{B}(\mathbf{X}^{m-1}) \cdot \mathbf{Z}\sqrt{\Delta t}, \tag{29}$$

where exponent m is the numerical step number, $\mathbf{X}^m$ is the three-dimensional position vector at time level $m\Delta t$, $\mathbf{A}(\mathbf{X}^{m-1})$ is the absolute forcing vector evaluated at $\mathbf{X}^{m-1}$ (i.e., a function of the velocity distribution), $\mathbf{B}(\mathbf{X}^{m-1})$ is a deterministic scaling second-order tensor evaluated at $\mathbf{X}^{m-1}$ (i.e., a function of the dispersion coefficient), and $\mathbf{Z}$ is a vector of three independent normally distributed random numbers with zero mean and unit variance. The terms of the diagonal second-order tensor $\mathbf{B}(\mathbf{X}^{m-1})$ are equal to $\sqrt{2D}$ (Ahlstrom et al. [41]).

The two-dimensional particle tracking equations for the uniform aperture fracture examined in this work can be written as

$$x^m = x^{m-1} + U_{\max}\left[1 - 4\left(\frac{z^{m-1}}{b}\right)^2\right]\Delta t + Z_1\sqrt{2\mathcal{D}\Delta t}, \tag{30}$$

$$z^m = z^{m-1} + Z_2\sqrt{2\mathcal{D}\Delta t}. \tag{31}$$

Using the effective velocity and dispersion coefficient derived in this work, the preceding two-dimensional particle tracking equations may be replaced by a one-dimensional particle tracking equation:

$$x^m = x^{m-1} + U_{\text{eff}}\Delta t + Z_1\sqrt{2D_{\text{eff}}\Delta t}. \tag{32}$$

Particles encountering the wall are reflected as a mirror image (James and Chrysikopoulos [33]).

Breakthrough curves generated for both the one- and two-dimensional particle tracking algorithms were indistinguishable from a breakthrough curve obtained by the analytical

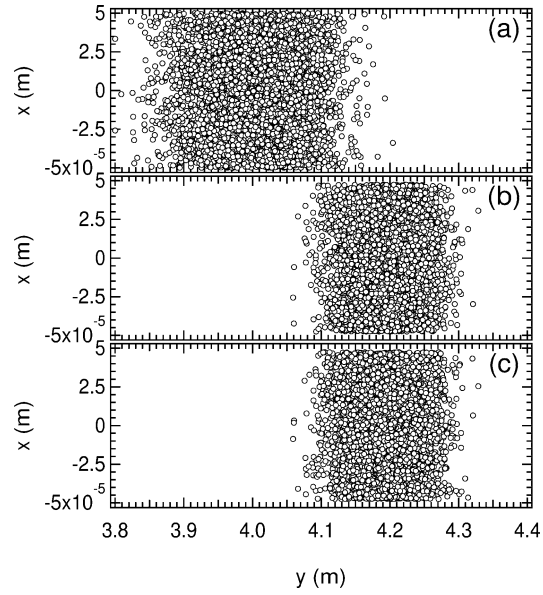

Fig. 5. Snapshots of a 5,000-particle plume with (a) infinitesimally small diameter determined by a two-dimensional particle tracking algorithm; (b) diameter $d_p = 5 \times 10^{-6}$ m determined by a two–dimensional particle tracking algorithm; and (c) diameter $d_p = 5 \times 10^{-6}$ m determined by a one-dimensional particle tracking algorithm employing the derived effective parameters (here $t = 70$ days, $b = 1 \times 10^{-4}$ m, $U_{\max} = 1 \times 10^{-6}$ m/s, and $T = 288.15$ K).

solution provided by Carslaw and Jaeger [42, p. 258],

$$\bar{n}(x,t) = \frac{n_0}{(4\pi D_{\text{eff}} t)^{1/2}} \exp\left[-\frac{(x - U_{\text{eff}} t)^2}{4 D_{\text{eff}} t}\right], \tag{33}$$

where n_0 is the initial number of particles introduced into the fracture per cross-sectional area of the fracture (James [43]). Note that (33) is the analytical solution to (18) subject to an instantaneous particle injection described by $\bar{n}(\xi, 0) = n_0 \delta(\xi)$ and $\bar{n}(\infty, t) = 0$, where δ is the Dirac delta function, with ξ replaced by $x - U_{\text{eff}} t$.

Snapshots of particle tracking simulations for both infinitesimally small and finite-sized particles are presented in Fig. 5. Results are obtained after approximately 70 days of travel time using a time step of $\Delta t = 100$ s through a fracture with aperture $b = 1 \times 10^{-4}$ m and centerline velocity of $U_{\max} = 1 \times 10^{-6}$ m/s. Figure 5a is a snapshot of two-dimensional particle tracking results for infinitesimally small particles ($\mathcal{D} = 8.41 \times 10^{-14}$ m^2/s). Figure 5b presents two-dimensional particle tracking results for particles with diameter $d_p = 5 \times 10^{-6}$ m (5% of the fracture aperture) and diffusion coefficient determined by the Stokes–Einstein equation. Figure 5c is a snapshot from the one-dimensional particle tracking algorithm based on the effective parameters derived in this work for particles with finite diameter ($d_p = 5 \times 10^{-6}$ m). It should be noted that the z-location of each particle across the fracture in Fig. 5c was randomly selected after the x locations of the particles in the plume were determined. Comparing Fig. 5a with Figs. 5b and 5c, two important features are evident. First, the mean particle locations for the particle plumes in Figs. 5b and 5c are greater than the mean particle location in Fig. 5a due to the increased average particle velocity for the plumes of finite-sized particles as determined by (3). Second, the spread of the particle plumes in Figs. 5b and 5c is less than that in Fig. 5a because the finite size of the particles reduces the effective dispersion of the particle plume according to (19). Certainly, the particle tracking results show that the finite size of the particles do indeed affect the transport behavior of a particle plume. The snapshots of the particle plumes in Figs. 5b and 5c show indistinguishable characteristics, suggesting that the two-dimensional particle tracking equations can be replaced by the more computationally efficient one-dimensional particle tracking equation that employs the effective parameters.

7. Summary

In this work an effective velocity (3) and an effective dispersion coefficient (19) for finite-sized, spherical, particles traveling in a uniform aperture fracture are derived. The slowly flowing carrier fluid forms a parabolic velocity profile within the fracture. Because particle–wall overlap is not allowed, and because a particle is assumed to flow at a velocity equal to that found near its centroid, the size of a particle physically excludes it from the slowest moving portion of the velocity profile located at the fracture walls. While this size exclusion serves to increase the effective travel velocity of a particle plume, it also decreases its effective dispersion coefficient. The effective dispersion coefficient derived here is found to be similar in form to the Taylor dispersion coefficient. In fact, in the limit of a particle diameter becoming infinitesimally small, the newly derived effective dispersion coefficient reduces to the classic Taylor dispersion coefficient. Extension of the parallel plate results to a uniform tube show similar particle behavior. Although other investigators have derived expressions for U_{eff} and D_{eff} applicable to particle transport in cylindrical tubes, the effective parameters derived in this work for particle transport in fractures with uniform aperture are unique. A particle tracking analysis is presented to compare the results between the transport of particles that are either infinitesimally small or of finite diameter. The results presented in this work suggest that the finite size of constituent particles increases the effective plume velocity and decreases the overall spreading of a particle plume.

Acknowledgments

Sandia is a multiprogram laboratory operated by Sandia Corporation, a Lockheed Martin Company, for the United States Department of Energy under Contract DE-AC04-94AL85000.

Appendix A. Nomenclature

A absolute forcing vector (L t^{-1})

b fracture aperture (L)
$\mathbf{B}$ deterministic scaling tensor ($\mathrm{L\,t^{-1/2}}$)
C integration constant ($\mathrm{L^{-4}}$)
d_p particle diameter (L)
D dispersion coefficient ($\mathrm{L^2\,t^{-1}}$)
D_{eff} effective dispersion coefficient for a plume of finite-sized particles ($\mathrm{L^2\,t^{-1}}$)
D_{Taylor} Taylor dispersion coefficient for a plume of infinitesimally small particles ($\mathrm{L^2\,t^{-1}}$)
$\mathcal{D}$ molecular diffusion coefficient ($\mathrm{L^2\,t^{-1}}$)
$\bar{J}$ average axial flux of particles relative to the moving coordinate ξ ($\mathrm{L^{-2}\,t^{-1}}$)
F hydrodynamic correction factor for wall effects (–)
k Boltzmann's constant ($\mathrm{M\,L^2\,t^{-2}\,T^{-1}}$)
m time step number (–)
n number concentration of particles per unit volume of interstitial fluid ($\mathrm{L^{-3}}$)
$\bar{n}$ average number concentration of particles per unit volume of interstitial fluid across the fracture ($\mathrm{L^{-3}}$)
n_0 initial number of particles introduced into the fracture per cross-sectional area of the fracture ($\mathrm{L^{-2}}$)
n_{cl} number concentration of particles per unit volume of interstitial fluid at the centerline of a fracture ($\mathrm{L^{-3}}$)
r radial distance from the center of a cylindrical tube (L)
R radius of a cylindrical tube (L)
t time (t)
Δt time step (t)
T absolute temperature of the interstitial fluid (T)
$u(z)$ local interstitial fluid velocity ($\mathrm{L\,t^{-1}}$)
$u_\xi(z)$ velocity defect, equal to $u(z) - U_{\mathrm{eff}}$ ($\mathrm{L\,t^{-1}}$)
$\overline{U}$ mean velocity of the interstitial fluid ($\mathrm{L\,t^{-1}}$)
U_{eff} effective velocity of a particle ($\mathrm{L\,t^{-1}}$)
U_{max} maximum interstitial fluid velocity along the centerline in the x-direction ($\mathrm{L\,t^{-1}}$)
x coordinate along the fracture length (L)
$\mathbf{X}$ three-dimensional position vector (L)
z coordinate perpendicular to the fracture (L)
Z_1, Z_2 randomly generated normally distributed number with zero mean and unit variance (–)
$\mathbf{Z}$ three-dimensional vector of randomly generated normally distributed numbers with zero mean and unit variance (–)
α constant in the hydrodynamic correction factor (–)
β constant in the hydrodynamic correction factor (–)
δ Dirac delta function (–)
η dynamic viscosity of the interstitial fluid ($\mathrm{M\,L^{-1}\,t^{-1}}$)
ξ coordinate transformation, equal to $x - U_{\mathrm{eff}}t$ (L)

References

[1] G.I. Taylor, Proc. R. Soc. London Ser. A 219 (1953) 186–203.
[2] R. Aris, Proc. R. Soc. London Ser. A 235 (1956) 67–77.
[3] R. Sankarasubramanian, W.N. Gill, Proc. R. Soc. London Ser. A 333 (1974) 115–132; correction, Proc. R. Soc. London Ser. A 341 407–408.
[4] L.E. Johns, A.E. DeGance, Chem. Eng. Sci. 30 (1975) 1065–1067.
[5] H. Brenner, Physicochem. Hydrodynam. 1 (1980) 91–123.
[6] H. Brenner, Physicochem. Hydrodynam. 3 (1982) 133–157.
[7] M. Shapiro, H. Brenner, Chem. Eng. Sci. 41 (6) (1986) 1417–1433.
[8] M. Shapiro, H. Brenner, AIChE J. 33 (7) (1987) 1155–1167.
[9] M. Shapiro, H. Brenner, Chem. Eng. Sci. 43 (3) (1988) 551–571.
[10] B. Berkowitz, J. Zhou, Water Resour. Res. 32 (4) (1996) 901–913.
[11] P. Grindrod, J. Contam. Hydrol. 13 (1993) 167–181.
[12] P. Grindrod, The Theory and Applications of Reaction–Diffusion Equations: Patterns and Waves, 2nd ed., Oxford Univ. Press, Oxford, 1996.
[13] D.H. Tang, E.O. Frind, E.A. Sudicky, Water Resour. Res. 17 (3) (1981) 555–564.
[14] E.A. Sudicky, E.O. Frind, Water Resour. Res. 18 (6) (1982) 1634–1642.
[15] J. Cormenzana, Water Resour. Res. 36 (2000) 1339–1346.
[16] A. Abdel-Salam, C.V. Chrysikopoulos, Adv. Water Resour. 17 (1994) 283–296.
[17] C.V. Chrysikopoulos, A. Abdel-Salam, Colloids Surf. A Physicochem. Eng. Aspects 121 (1997) 189–202.
[18] P.A. Smith, C. Degueldre, J. Contam. Hydrol. 13 (1993) 143–166.
[19] J.S. Contardi, D.R. Turner, T.M. Ahn, J. Contam. Hydrol. 47 (2001) 323–333.
[20] A. Abdel-Salam, C.V. Chrysikopoulos, J. Hydrol. 165 (1995) 261–281.
[21] A. Abdel-Salam, C.V. Chrysikopoulos, Transp. Por. Media 20 (3) (1995) 197–221.
[22] H. Brenner, L.J. Gaydos, J. Colloid Interface Sci. 58 (1977) 312–356.
[23] R.W. Fox, A.T. McDonald, Introduction to Fluid Mechanics, 5th ed., Wiley, New York, 1998.
[24] R.B. Bird, W.E. Stewart, E.N. Lightfoot, Transport Phenomena, Wiley, New York, 1960.
[25] J.H. Kessler, J.R. Hunt, Water Resour. Res. 30 (4) (1994) 1195–1206.
[26] E.A. DiMarzio, C.M. Guttman, J. Chromatogr. 55 (1971) 83.
[27] J.L. Anderson, J.A. Quinn, Biophys. J. 14 (1974) 130–150.
[28] T.G.M. van de Ven, Colloidal Hydrodynamics, Academic Press, London, 1989.
[29] A.J. Goldman, R.G. Cox, H. Brenner, Chem. Eng. Sci. 22 (1967) 653–660.
[30] M.E. O'Neill, K. Stewartson, J. Fluid Mech. 27 (4) (1967) 705–724.
[31] S.L. Goren, M.E. O'Neill, Chem. Eng. Sci. 26 (1971) 325–338.
[32] C.V. Chrysikopoulos, P.K. Kitanidis, P.V. Roberts, Transp. Por. Media 7 (1992) 163–185.
[33] A.F.B. Thompson, A.L. Schafer, R.W. Smith, Water Resour. Res. 32 (4) (1996) 801–818.
[34] S.C. James, C.V. Chrysikopoulos, Water Resour. Res. 35 (3) (1999) 707–718.
[35] S.C. James, C.V. Chrysikopoulos, Water Resour. Res. 36 (6) (2000) 1457–1465.
[36] S.C. James, C.V. Chrysikopoulos, Chem. Eng. Sci. 56 (23) (2001) 6535–6543.
[37] P.W. Reimus, S.C. James, Chem. Eng. Sci. 57 (21) (2002) 4429–4434.
[38] C.V. Chrysikopoulos, S.C. James, Transp. Por. Media 51 (2003) 191–210.
[39] P.K. Kitanidis, Water Resour. Res. 30 (11) (1994) 3225–3227.
[40] A.F.B. Thompson, L.W. Gelhar, Water Resour. Res. 26 (10) (1990) 2541–2562.
[41] S.W. Ahlstrom, H.P. Foote, R.C. Arnett, C.R. Cole, R.J. Serne, Multicomponent mass transport model: theory and numerical implementation (discrete-parcel-random-walk version), Tech. Rep., Atlantic Richfield Hanford Company, Richland, WA, 1977.
[42] H.S. Carslaw, J.C. Jaeger, Conduction of Heat in Solids, 2nd ed., Oxford Univ. Press, Oxford, 1988.
[43] S.C. James, Polydisperse Colloid Transport in Fractured Media, Ph.D. thesis, Univ. of California, Irvine, 2001.